J|A|C|S
ARTICLES
Published on Web 03/20/2004

Nano-Architectural Silica Thin Films with Two-Dimensionally Connected Cagelike Pores Synthesized from Vapor Phase

Shunsuke Tanaka,[†] Norikazu Nishiyama,*[,†] Yoshiaki Oku,[‡] Yasuyuki Egashira,[†] and Korekazu Ueyama[†]

Contribution from the Division of Chemical Engineering, Graduate School of Engineering Science, Osaka University, 1-3 Machikaneyama, Toyonaka, Osaka 560-8531 Japan, and MIRAI Project, Association of Super-Advanced Electronics Technology (ASET), AIST Tsukuba West 7, 16-1 Onogawa, Tsukuba, Ibaraki 305-8569 Japan

Received October 28, 2003; E-mail: nisiyama@cheng.es.osaka-u.ac.jp.

Abstract: Novel mesostructured silica thin films were prepared on a Si substrate by a vapor-phase synthesis. Vapor of tetraethoxysilane (TEOS) was infiltrated into a surfactant film consisting of a poly(ethylene oxide)−poly(propylene oxide)−poly(ethylene oxide) triblock copolymer. Nanophase transition from a lamellar structure to a two-dimensional cage structure of a silica−surfactant nanocomposite was found under vapor infiltration. The rearrangement into the cage structure implies high mobility of the silica−surfactant composites in solid phase. The silica thin films have two-dimensionally connected cagelike mesopores and are isotropic parallel to the film surface. The structure of pores of the films is advantageous for next-generation low-k films. The mesoporous structure has a large lattice parameter *d* of ∼102 Å, silica layer thickness of ∼58 Å, pillar diameter in the middle of ∼60 Å, pore size of ∼72 Å, BET surface area of ∼729 m^2/g, and pore volume of ∼1.19 cm^3/g. The films synthesized by the vapor infiltration show a lower concentration of residual Si−OH groups compared to the films prepared by a conventional sol−gel method. The films show high thermal stability up to 900 °C and high hydrothermal stability. This method is a simpler process than conventional sol−gel techniques and attractive for mass production of a variety of organic−inorganic composite materials and inorganic porous films.

Introduction

Preparation of thin films of mesoporous materials[1−8] has attracted considerable attention because of their possible applications in the fields of separations, chemical sensors, optical devices, and electronic devices such as low-k dielectric films. The mesoporous materials contain several unique structures: lamellar (MCM-50[9]), cubic *Pm3n* (SBA-1[10]), cubic *Ia3d* (MCM-48[9]), two-dimensional hexagonal *P6m* (FSM-16,[11] MCM-41,[9] SBA-3,[10] and SBA-15[12]), and three-dimensional hexagonal $P6_3/mmc$ (SBA-2[10]). The desired mesostructures of the silica materials have conventionally been obtained by controlling the composition and pH of a precursor solution and synthetic time and temperature. The geometric structures are based on the idea of a surfactant packing parameter.[13] Moreover, several phase transitions from one kind of mesostructure to another are found under drying[13,14] and hydrothermal conditions.[15]

In contrast, we have first found phase transition of surfactant−silicate nanocomposites under vapor-phase synthesis.[16] Cetyltrimethylammonium bromide (C_{16}TAB) films on a Si substrate were treated with tetraethoxysilane (TEOS) and tetramethoxysilane (TMOS). The obtained films have hexagonally arranged pore channels that run parallel to the film surface. However, when the films are used as electric devices, the structure of pores of the films should be isotropic parallel to the surface in some cases. In vapor-phase method, selection of surfactant is the most important factor to determine the porous structure similarly to

* To whom correspondence should be addressed. Phone: +81-6-6850-6256. Fax: +81-6-6850-6256.
[†] Osaka University.
[‡] Association of Super-Advanced Electronics Technology (ASET).

(1) Ogawa, M. *J. Am. Chem. Soc.* **1994**, *116*, 7941−7942.
(2) Aksay, I. A.; Trau, M.; Manne, S.; Honma, I.; Yao, N.; Zhou, L.; Fenter, P.; Eisenberger, P. M.; Gruner, S. M. *Science* **1996**, *273*, 892−898.
(3) Yang, H.; Coombs, N.; Sokolov, I.; Ozin, G. A. *Nature* **1996**, *381*, 589−592.
(4) Yang, H.; Kuperman, A.; Coombs, N.; Mamich-Afara, S.; Ozin, G. A. *Nature* **1996**, *379*, 703−705.
(5) Yang, H.; Coombs, N.; Sokolov, I.; Ozin, G. A. *J. Mater. Chem.* **1997**, *7*, 1285−1290.
(6) Nishiyama, N.; Koide, A.; Egashira, Y.; Ueyama, K. *Chem. Commun.* **1998**, 2147−2148.
(7) Lu, Y.; Ganguli, R.; Drewien, C. A.; Anderson, M. T.; Brinker, C. J.; Gong, W.; Guo, Y.; Soyez, H.; Dunn, B.; Huang, M. H.; Zink, J. I. *Nature* **1997**, *389*, 364−368.
(8) Sellinger, A.; Weiss, P. R.; Nguyen, A.; Lu, Y.; Assink, R. A.; Gong, W.; Brinker, C. J. *Nature* **1998**, *394*, 256−260.
(9) Vartuli, J. C.; Schmitt, K. D.; Kresge, C. T.; Roth, W. J.; Leonowicz, M. E.; McCullen, S. B.; Hellring, S. D.; Beck, J. S.; Schlenker, J. L.; Olson, D. H.; Sheppard, E. W. *Chem. Mater.* **1994**, *6*, 2317−2326.
(10) Huo, Q.; Leon, R.; Petroff, P. M.; Stucky, G. D. *Science* **1995**, *268*, 1324−1327.
(11) Inagaki, S.; Fukushima, Y.; Kuroda, K. *J. Chem. Soc. Chem. Commun.* **1993**, 680−682.
(12) Zhao, D.; Feng, J.; Huo, Q.; Melosh, N.; Fredrickson, G. H.; Chmelka, B. F.; Stucky, G. D. *Science* **1998**, *279*, 548−552.
(13) Grosso, D.; Babonneau, F.; Soler-Illia, G. J. A. A.; Albouy, P.; Amenitsch, H. *Chem. Commun.* **2002**, 748−749.
(14) Liu, M.-C.; Sheu, H.-S.; Cheng, S. *Chem. Commun.* **2002**, 2854−2855.
(15) Huo, Q.; Margolese, D. I.; Stucky, G. D. *Chem. Mater.* **1996**, *8*, 1147−1160.
(16) Nishiyama, N.; Tanaka, S.; Egashira, Y.; Oku, Y.; Ueyama, K. *Chem. Mater.* **2003**, *15*, 1006−1011.

10.1021/ja039267z CCC: $27.50

the sol−gel method. In this report, we show a novel mesostructured film whose porous structure was isotropic parallel to the film surface. The porous structure of the films was determined by X-ray diffraction (XRD), field emission scanning electron microscope (FE-SEM), and transmission electron microscope (TEM) observations. The amount of Si−OH groups, thermal stability, and hydrothermal stability were determined by Fourier transform infrared spectroscopy (FTIR), XRD, and N_2 adsorption/desorption measurements.

Experimental Section

Mesostructured silica films were prepared as follows: A silicon wafer was cut into 5 × 5 cm pieces and used as a substrate. Nonionic poly(ethylene oxide)−poly(propylene oxide)−poly(ethylene oxide) amphiphilic triblock copolymer ($EO_{106}PO_{70}EO_{106}$; Pluronic F127) was used as a templating agent. The surfactant film was prepared on the silicon wafer by spin-coating using a solution of Pluronic F127, ethanol (EtOH), and deionized water (the mole ratios: 0.03 Pluronic F127: 100 EtOH: 100 H_2O). The surfactant film was placed vertically in a closed vessel (200 cm^3) along with a separate, small amount of TEOS and HCl (5 N). The vessel was then placed in an oven at 90 °C for 60 min. Thus, the surfactant film was exposed to a saturated TEOS vapor under autogenous pressure. The film was calcined at 400 °C in air for 5 h with a heating rate of 1 °C/min.

The products were identified by XRD patterns recorded on a Philips X′ Pert-MPD using Cu-Kα radiation with $\lambda = 1.5418$ Å in the θ-2θ scan mode. FTIR spectra of the products were recorded in the 500−3800 cm^{-1} range using a FTIR-8200PC spectrometer (Shimadzu Co.) at 4 cm^{-1} resolution. FE-SEM images were recorded on a Hitachi S-5000L microscope at an acceleration voltage of 21 kV. No coating was carried out for the samples before the FE-SEM measurements. TEM images of a calcined mesoporous silica film were recorded on a Hitachi H9000 electron microscope at an acceleration voltage of 300 kV. The N_2 adsorption/desorption isotherms of products were measured at 77 K using an AUTOSORB-1 instrument (Quantachrome Co.). The measurements were performed with the film on the Si substrate and powdery sample which was peeled from the Si substrate. The pore size distributions were calculated using the BJH model from the desorption branch. The pore volume was determined from the adsorption branch of the N_2 isotherm curve at $P/P_0 = 0.983$. The surface area was calculated by the BET method.

The mesoporous silica films were heated in air at 650 and 900 °C for 3 h to determine their thermal stability. The hydrothermal stability of the films was examined by immersing the films in water at 180 °C in a closed vessel for 3 h.

Results and Discussion

Figure 1A shows XRD pattern of a surfactant film before contacting TEOS vapor, suggesting that the surfactant film does not have ordered periodic structure. The XRD pattern of a surfactant−silicate film after vapor infiltration is shown in Figure 1B, which has a large 100 reflection (the lattice spacing $d = 103.2$ Å). Figure 1C shows the XRD pattern of the mesoporous silica film calcined at 400 °C. The 100 reflection peak hardly shifted after calcination (the lattice spacing $d = 102.0$ Å), indicating that contraction of the ordered structure did not occur during calcination. The full-width at half-maximum (fwhm) of the diffraction peak did not change (∼0.06°), indicating that the mesostructure remained uniform.

Figure 2 presents N_2 adsorption/desorption isotherms of the mesoporous silica film which was peeled from the Si substrate. The pore size distribution was obtained using the BJH model for the desorption isotherm (shown as an inset in Figure 2). At

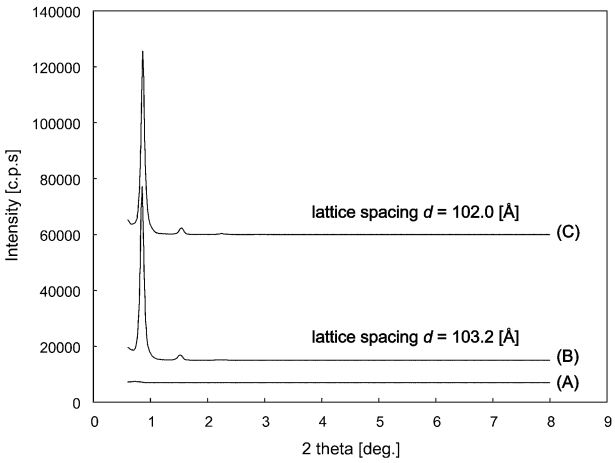

Figure 1. XRD patterns of (A) a surfactant film, (B) a mesostructured silica film after vapor infiltration, and (C) a calcined mesoporous silica film. Calcination temperature was 400 °C.

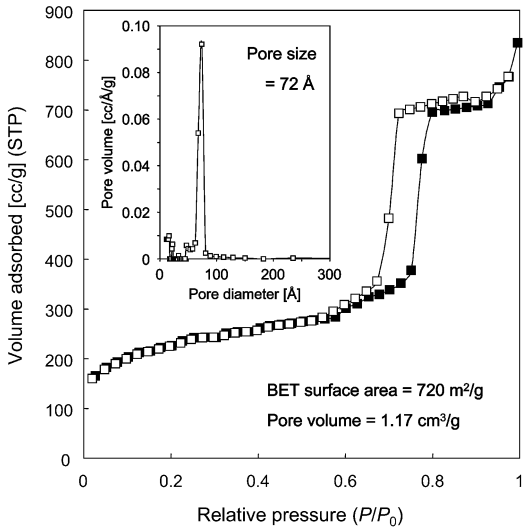

Figure 2. Nitrogen adsorption (■)/desorption (□) isotherms and a pore size distribution for a calcined mesoporous silica film prepared by vapor infiltration. The film was peeled from a Si substrate. STP, standard temperature and pressure.

a relative N_2 pressure of 0.7−0.8, a steep increase in the amount of adsorbed N_2 with a hysteresis loop corresponds to the filling of ordered mesopores. The BET surface area of the mesoporous silica film, calculated by assuming the covered area by nitrogen molecules as 0.162 nm^2, was 720 m^2/g. The mesoporous silica film shows a sharp pore size distribution, with a pore diameter of 72 Å.

The FTIR spectra of mesostructured silica films are shown in Figure 3. The bands at about 1100 and 2900 cm^{-1} observed in the spectrum of the surfactant film (Figure 3A) are ascribed to the stretching vibrations of the -CH_2OCH_2- and the C−H groups, respectively. After a vapor infiltration using TEOS vapor, the Si−O−Si antisymmetric stretching modes appear at about 1080 and 1180 cm^{-1} (Figure 3B). Complete removal of surfactant molecules by calcination at 400 °C was confirmed by the spectrum of the calcined silica film in Figure 3C. The FTIR spectrum for a silica film obtained by a conventional sol−gel method (Figure 3D) shows a broad band at about 3500 cm^{-1}, which is assigned to physically adsorbed water and Si−OH groups. The narrow band observed at about 3700 cm^{-1} in Figure 3D is assigned to the free Si−OH groups. Conversely, the FTIR

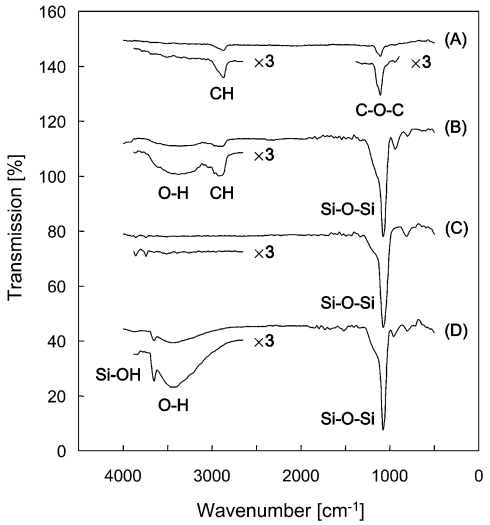

Figure 3. FTIR spectra of (A) a surfactant film, (B) a mesostructured silica-surfactant film after vapor infiltration, (C) a calcined film, and (D) a calcined mesoporous silica film synthesized by a conventional sol−gel method. Vapor infiltration was performed with TEOS and HCl vapors at 90 °C for 60 min.

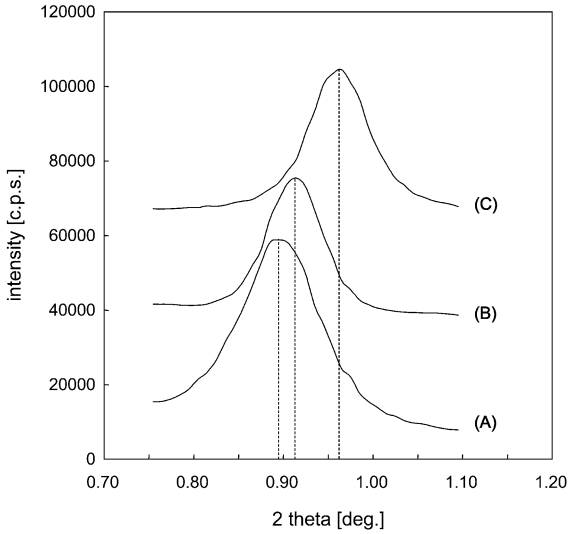

Figure 4. XRD patterns of (A) a mesoporous silica film after calcination at 400 °C and the same film heated at (B) 650 °C and (C) 900 °C for 3 h.

spectra for the films synthesized by vapor infiltration show that the concentration of residual Si−OH groups is extremely low even before calcination. The vapor infiltration process was conducted at high temperatures in the absence of aqueous solution, which is an advantageous synthetic condition to the complete condensation of the Si−OH groups. The densified silica wall by successive penetration of TEOS molecules and incorporation in the silicate network has high structural stability and hardly contracts under calcination process.

Thermal and hydrothermal stability of the mesoporous silica thin film were investigated. Figure 4 shows XRD patterns of the mesoporous silica film after calcination at 400 °C and the same film heated at 650 and 900 °C for 3 h. The 100 reflection peak shifted with a rise in temperature. Shrinkage percentages of the calcined film after heating at 650 and 900 °C were calculated to be 2.4 and 9.4%, respectively. However, peak intensity did not change, indicating that periodic structure was retained after heating. N_2 adsorption/desorption measurements were performed using films attached with the Si substrate (see

Table 1. Effect of Thermal and Hydrothermal Treatments on the Lattice Spacing *d*, BET Surface Area, Pore Volume, and Pore Size of the Calcined Mesoporous Silica Thin Films

treatment conditions[a]	*d* (Å)	BET surface area (m^2/g)	pore volume (cm^3/g)	pore size (Å)
400°C, in air	101	729	1.19	68
650°C, in air	99	716	1.15	68
900°C, in air	92	693	1.04	63
180°C, in water	101	726	1.12	68

[a] The films were treated for 3 h.

Supporting Information, Figures S1 and S2). The results from this method are in reasonable agreement with those from the measurements with powdery samples peeled from the Si substrate. Fluctuation of the data was observed because the sample weight was small (0.43 mg). Weight of the films on the Si substrate was estimated from the calculation of the following formula: weight of the films = area of the films (62.5 cm^2) × thickness of the films (80×10^{-7}cm) × density of the films (0.86 g/cm^2). The density of the films was calculated using the pore volume (1.17 cm^2/g) of the powdery sample which was peeled from the Si substrate. Table 1 summarizes the results of the pore structure analysis after the thermal and hydrothermal treatments: the lattice spacing *d*, BET surface area, pore volume, and pore diameter of the mesoporous silica. The pore volume was slightly decreased with a rise in heating temperature. The pore size of the film heated at 900 °C shrunk about 8%, although no shrinkage was observed in the pore size after heating at 650 °C.

The pore size distributions of the mesoporous silica film were estimated before and after immersing in water at 180 °C in a closed vessel for 3 h (see Supporting Information, Figure S3). The pore size, BET surface area, and pore volume were summarized in Table 1. The results show high hydrothermal stability of mesoporous silica film prepared from vapor phase. Hydrothermal stability seems to be related to hydrophobicity of the film. The surface of films is thought to be more hydrophobic than the ones by the sol−gel method because of a low concentration of the Si−OH groups. If the films are used as low-k film, the low adsorption capacity of water is an attractive feature because the dielectric constant of water is very large ($k = 81$).

Figure 5A,B shows the FE-SEM images of the cross-section of the mesoporous silica film. On the basis of the FE-SEM observation, a plausible structure of the mesoporous silica film on the silicon substrate was illustrated in Figure 5C. The parts marked with A and B correspond to the observed positions shown in Figure 5A,B, respectively. A unique architectural structure was found in Figure 8A. After the edge of the silica film was peeled from the Si substrate, hexagonally arranged stubbed pillars were found on the substrate surface. The mesoporous silica film consists of layered silica parallel to the film surface with periodic pillars. The mesostructures of the thin film are summarized in Figure 5D: the lattice spacing *d* of 102 Å, silica layer thickness of 58 Å, and pillar diameter in the middle of 60 Å. FE-SEM observations strongly support the results of XRD analysis in Figure 1. The film has eight layers and was about 80-nm thick. The pores at the film−substrate interface are hemisphere in shape. Nanopores look like ellipsoidal structures whose diameter along the lateral axis (95 Å) is longer than the one along the longitudinal axis (44 Å).

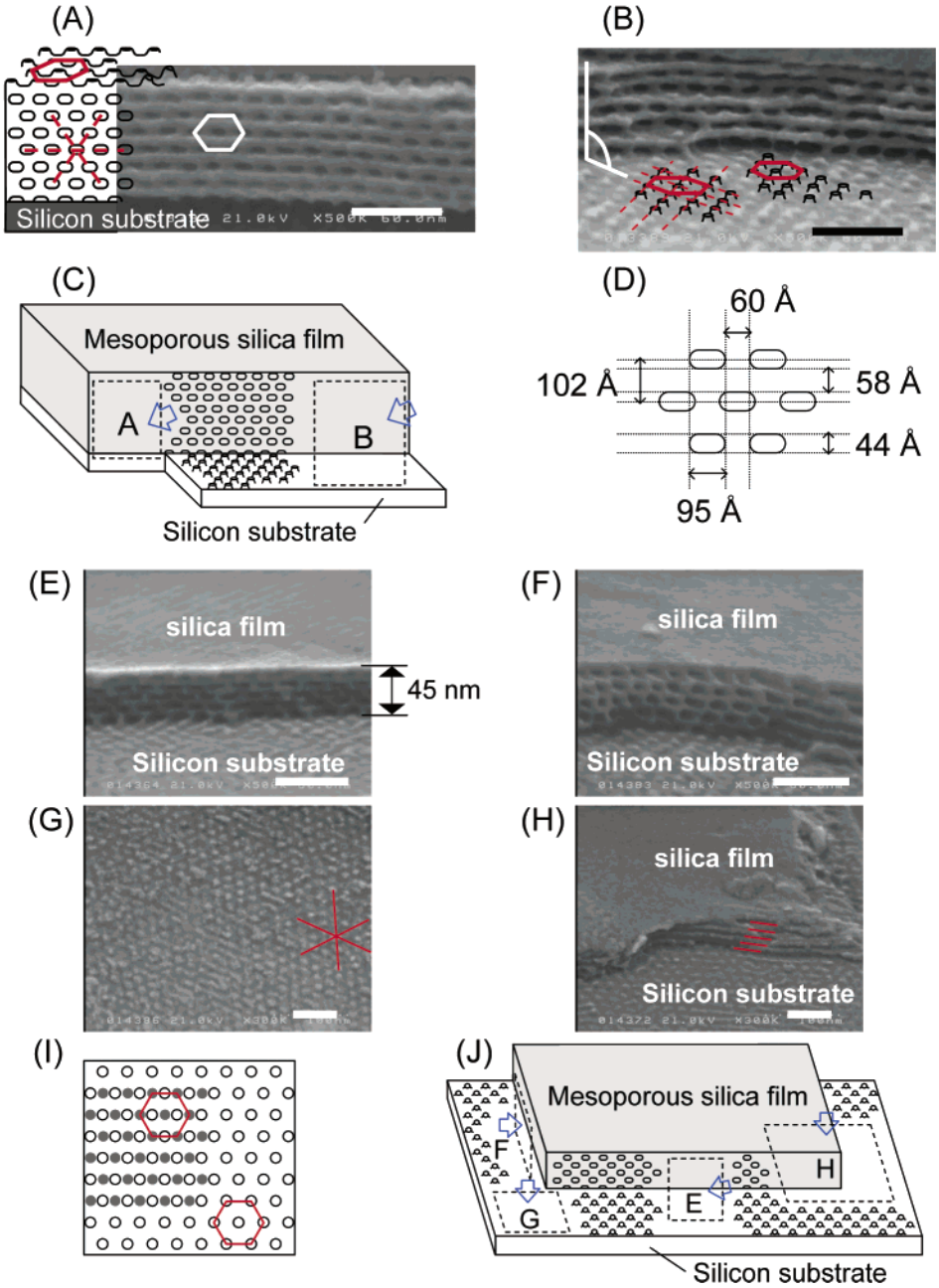

Figure 5. FE-SEM images of the cross-section of a calcined mesoporous silica film (scale bar; 600 Å). (A and B) The cross-section of the mesoporous silica film on the Si substrate. (C and D) A layout of the plausible mesoporous structure based on the FE-SEM observation (A and B). FE-SEM images of (E and F) the cross-section and (G and H) top of a calcined mesoporous silica film. (I) A graphical illustration of the arrangement of the pillars observed from the top. Open and closed circles represent pillars under the first and the second layers, respectively. (J) A layout of the plausible mesoporous structure based on the FE-SEM observations (G and H).

Thinner mesoporous silica films were obtained using a solution with a low concentration of the surfactant. The molar ratios of precursor solution for surfactant films were 0.008 Pluronic F127: 100 EtOH: 100 H_2O. The vapor infiltration was performed for 30 min. FE-SEM observation of the film was performed from different directions (Figure 5E−H). A plausible structure of the mesoporous silica film on the silicon substrate was illustrated in Figure 5J. The parts marked with E, F, G, and H in Figure 5J correspond to the observed positions shown in Figure 5E−H, respectively. The film has five layers and was about 45-nm thick. Figure 5G,H shows the FE-SEM image of the Si surface where the film was peeled off. A graphical illustration of the arrangement of the pillars observed from the top was shown in Figure 5I. The positions of the pillars under the first and second layer were shown in open and closed symbols, respectively. Periodic pillars were arranged hexagonally. The pillar size in the middle was estimated as about 60 Å wide. The repeated distance from pillar to pillar was estimated as about 102 Å.

The structure of pores of the films are advantageous for next-generation low-k films because (1) the electric property of the films are isotropic parallel to the film surface, and (2) the silica layers play a role as passivating films. Capping of the nanopores on the top surface, therefore, is not inevitable. Moreover, the

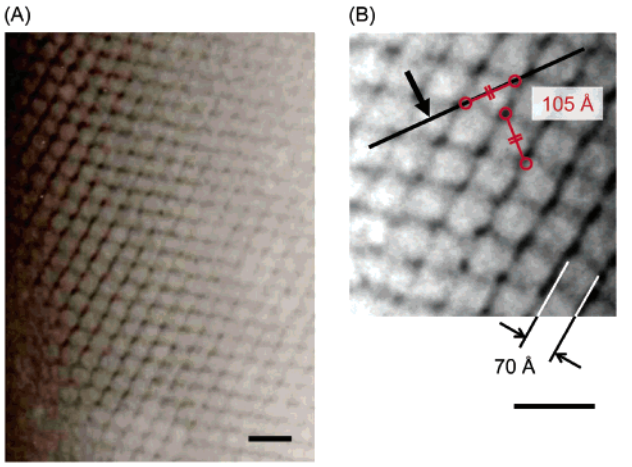

Figure 6. (A, B) TEM images of the calcined mesoporous silica thin film (Scale bar; 200 Å).

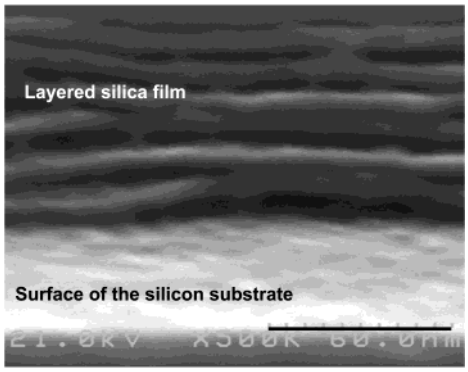

Figure 7. FE-SEM image of the cross-section of the layered silica film with few pillars (scale bar; 600 Å).

mesoporous silica films prepared by vapor-phase synthesis show superior characteristics, such as high structural stability under calcination and high hydrothermal stability.

TEM images of the mesoporous silica films peeled from the Si substrate are shown in Figure 6. The periodic porous structure was observed. Because the film thickness is at most 80 nm, the image was observed in the direction perpendicular to the film surface. The parts showing light and dark contrasts correspond to pores and pillars, respectively. The FE-SEM image in Figure 5A must be observed in the direction shown by an arrow in Figure 6B. The distance between pillars was in good agreement with the results of FE-SEM observation (Figure 5G).

Figure 7 shows the FE-SEM image of the cross-section of the film prepared in short synthetic time (~20 min). The layered silica has fewer pillars compared to those observed in Figure 5 (see Supporting Information, Figure S4). This result strongly supports the nanophase transition under vapor infiltration. The layered silica is first formed in the early stage of the vapor infiltration and then pillars are formed with increasing concentration of TEOS molecules in the film, resulting in the distortion to the longitudinal axis arises in the mesostructured silica films. We proposed a mechanism for the formation of mesostructured silica film under vapor infiltration in Figure 8. The TEOS molecules infiltrate into the layers of surfactant aggregation.

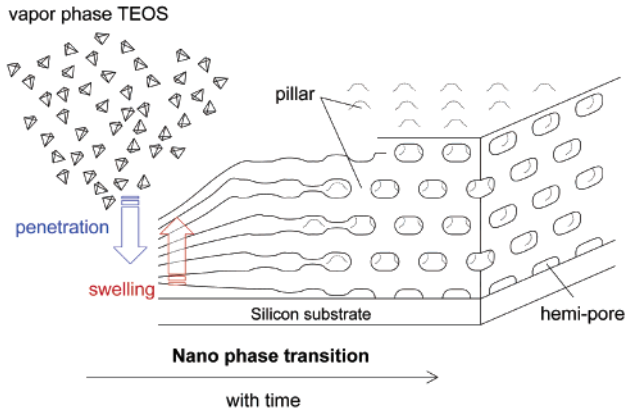

Figure 8. A graphical illustration of the proposed model for the formation of a mesoporous silica film on a Si substrate via vapor infiltration.

The TEOS molecules in the film interact with the hydrophilic PEO chain of surfactants and form TEOS−surfactant composites. As the TEOS molecules penetrate into the silica layers, the film is swollen and pillars grow up perpendicular to the silicate layer. The TEOS−surfactant composites dynamically rearrange to a two-dimensional cage structure. Simultaneously, the penetrating TEOS molecules react with the Si−OH groups, resulting in the densification of silica wall. This method contains competitive two processes: (1) the penetration of TEOS into the films and (2) the reaction of the Si−OH groups. The film thickness and the lattice spacing can be controlled by adjusting the rate of the two processes. The synthetic temperature, reactivity of silica sources, catalysts, and the thickness of surfactant films were important factors.

Conclusion

Novel mesoporous silica thin films were synthesized by a vapor infiltration technique. The mesostructured silica thin films have silicate layers with ordered pillars and are isotropic parallel to the film surface. The structure of pores of the films is advantageous for next-generation low-k films and other optoelectronic devices. The nanophase transition of TEOS−surfactant composites under vapor infiltration implies their high mobility and flexibility. The vapor-phase synthesis can be applied for organic−inorganic nanocomposites and mesoporous metal oxides other than silica and provides opportunities for the creation of new materials technologies.

Acknowledgment. This work was supported by the New Energy and Industrial Technology Development Organization (NEDO) under the Millennium Research for Advanced Information Technology (MIRAI) project. The authors wish to thank the GHAS laboratory and Mr. M. Kawashima (Osaka University) for FE-SEM measurements, and Prof. H. Mori and Dr. T. Sakata (Osaka University, Research Center for Ultrahigh Voltage Electron Microscopy) for TEM measurements.

Supporting Information Available: Detailed characterization data and additional FE-SEM images. This material is available free of charge via the Internet at http://pubs.acs.org.

JA039267Z